Shallow Water Flow through a Contraction

Benjamin Akers
Department of Mathematics, University of Wisconsin, U.S.A.

July 18, 2006

1 Introduction

Shallow water flows in channels are of interest in a variety of physical problems. These include river flow through a canyon, river deltas, and canals. Under certain conditions we can get large hydraulic jumps, or their moving counterparts bores, in the channel. There are a number of places where these bores are generated in rivers around the world, including the River Severn in England, and the Amazon in Brazil [6].

Figure 1: A surfer riding a tidal bore on the Amazon.

In this work, we will be concerned with the effect that geometry and flow rate have on the formation and stability of hydraulic jumps. The general setup is inspired by Al-Tarazi et al. [2] and Baines and Whitehead [4]. The motivations are to use the present study to investigate shallow water flow and also as a tool for comparison with the granular media flows studied in [2]. The idea being that this will lay a foundation for the study of mixed media flows.

The body of this report is divided into five sections. First we will present the one dimensional inviscid hydraulic theory. Then we will compare the inviscid theory with the experimental results. Next we will discuss some two dimensional and frictional effects. Finally, we will discuss some areas for future research and make some concluding remarks.

2 Experimental setup

We conducted a series of experiments in a linear flume with a flat bottom and piecewise linear cross section. Water flows through a sluice gate at the beginning of our channel, pours out of the end into a large reservoir, and is recirculated using pumps. The setup is shown in Figure 2.

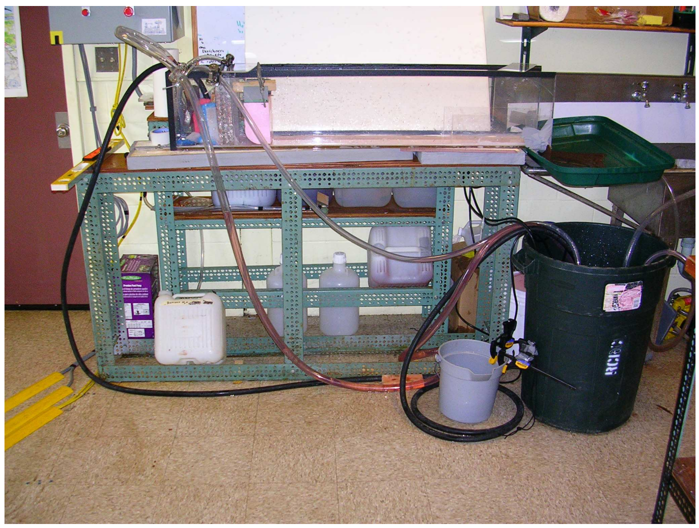

Figure 2: The experiments were done in a linear plexiglass flume, where water was recirculated using pumps in a large trash can, seen on the right, downstream of the contraction.

The flume had a 20 cm cross section, and was approximately 1.5 m in length. When all three of the pumps were in operation, we could generate a volume flux up to 4 liters/sec. For each experiment two plexiglass paddles, 30.5 cm long, are fixed at a given angle at the end of the channel. The flow rate is set by turning on the desired number of pumps and restricting the flow until the various flow states are observed. The flow rate is then measured using a bucket and a stopwatch at the end of the channel. In order to increase the accuracy of our flow measurement, the discharge was measured a minimum of five times and the mean of these measurements was taken as the flow rate. In each experiment the height of the fluid is measured by placing a thin ruler in the fluid parallel to the flow velocity and visually estimating the depth. Data was taken at a variety of nozzle widths and flow speeds. A schematic of the experimental setup is shown in Figure 3.

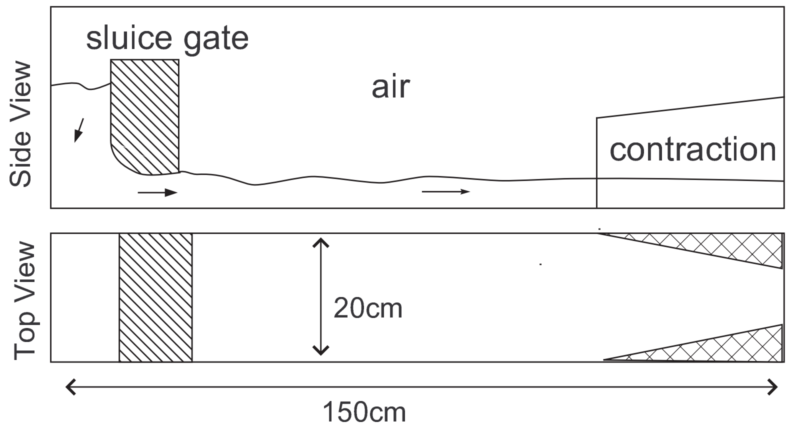

Figure 3: A sketch of the tank is given. The tank is piecewise linear, with paddles at the end to regulate the nozzle width.

3 One Dimensional Inviscid Flows

Here we will present the mathematical formulation of the problem of flow through a channel with a contraction. We will derive the governing equations from conservations laws and use these to give predictions for steady one dimensional (1-D) flows. Next, we will determine the necessary flow conditions for moving shocks, as well as for stationary shocks. Finally, we will derive a stability condition for steady shocks in a contraction.

3.1 Conservation Laws

Conservation of mass of a constant density fluid in a shallow channel can be written as

$$\frac{\mathrm{d}}{\mathrm{d}t}\int_{x_0}^{x_1}\int_0^{b(x)}\int_0^{h(x,y,t)}\rho dz dy dx = \int_0^{b(x)}\int_0^{h(x,y,t)}\rho\big(u(x_0,y,t)-u(x_1,y,t)\big)dz dy, \quad (1)$$

where the x-axis is measured down the centerline of the channel, x_0 and x_1 are arbitrary points on this axis, and t is time. If we use the divergence theorem on the integral on the right hand side, and take h and u to be independent of y this becomes

$$\int_{x_0}^{x_1}\left[\rho b(x)h(x,t)\right]_t + \left[\rho b(x)h(x,t)u(x,t)\right]_x dx = 0. \quad (2)$$

Since x_0 and x_1 are arbitrary we get that the argument of our integral must be equal zero pointwise

$$(bh)_t + (bhu)_x = 0. \quad (3)$$

Here u is the velocity, h the height of the free surface, b the width of the channel, and ρ the density of the fluid. Partial derivatives are written in two ways as $\partial_t(\cdot) = (\cdot)_t$ and so forth.

For water, ρ, is taken constant, and we therefore have dropped the ρ dependence from (3). We can also get a momentum equation using Newton's second law of motion

$$\frac{\mathrm{d}}{\mathrm{d}t}\int_{CV}\rho u(x,y,t)dV = \int_{CS}\rho u(x,y,t)^2\cdot\mathbf{n}dA + \int_{CV}FdV + \int_{CS}S\cdot\mathbf{n}dA, \tag{4}$$

where dA and dV are infinitesimal area and volume elements. To make the notation simpler we have omitted the bounds of our integrals, instead writing CV for an arbitrary control volume, and CS for the surface of that volume. If we make the assumption that the pressure forces are hydrostatic, then the acceleration in the vertical direction is negligible, and the body forces must balance the surface stress to give hydrostatic pressure $p - p_0 = \rho g(h-y)$ (see, e.g., [9]), where g is the acceleration due to gravity. We can use Stokes' theorem to turn (4) into a volume integral, and after assuming again $h = h(x,t), u = u(x,t)$ we obtain

$$(bhu)_t + (bhu^2)_x + \frac{1}{2}gb(h^2)_x = 0. \tag{5}$$

3.2 Smooth Hydraulic Flow

In this section, we are looking at flows which have reached a steady state. This allows us to simplify (3) and (5) into

$$(bhu)_x = 0 \tag{6a}$$
$$(bhu^2)_x + \frac{1}{2}gb(h^2)_x = 0. \tag{6b}$$

When the solutions are smooth we can expand the derivatives in (6b) to get

$$(\frac{1}{2}u^2 + gh)_x = 0. \tag{7}$$

Next, introduce the local Froude number, $F = u/\sqrt{gh}$. Eliminating u_x from (6) yields

$$-\frac{u^2}{gh}(bh)_x + bh_x = 0 \tag{8}$$

or

$$(1-F^2)bh_x = F^2hb_x. \tag{9}$$

Thus we see that if $F = 1$ then b must be stationary, or in our case at a minimum. Note that the converse is not true, when $b_x = 0$ we have that $F = 1$ or $h_x = 0$ but not necessarily both. We will define the flow to be subcritical when $F < 1$ and supercritical when $F > 1$. Equation (9) tells us that for smoothly contracting $b(x)$, the subcritical fluid flow must have a minimum in h at the nozzle. Similarly, supercritical flow must have a maximum at the nozzle, see Figure 4.

Next we will examine for what range of far field Froude numbers $F_0 = u_0/\sqrt{gh_0}$ and contraction ratios $B = b_c/b_0$, we can have smooth solutions. Since the flow is smooth we can follow the two constants of the flow

$$Q = b_0h_0u_0 = b_ch_cu_c \tag{10a}$$
$$E = u_0^2/2 + gh_0 = u_c^2/2 + gh_c. \tag{10b}$$

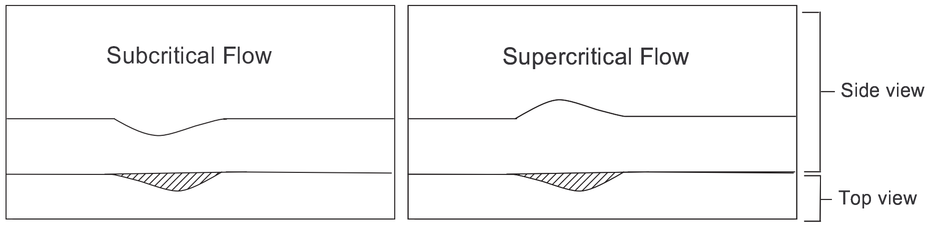

Figure 4: The shape of the free surface of supercritical and subcritical smooth flow through a nozzle. Both the top view and a profile are shown in this figure.

If we non-dimensionalize, $H = h_c/h_0$ and $B = b_c/b_0$, then (10) is equivalent to the cubic polynomial, $p(H) = 0$, with parameters B and F_0, where

$$P(H) = H^3B^2 - (\frac{1}{2}F_0^2 + 1)B^2H^2 + \frac{1}{2}F_0^2 = 0. \tag{11}$$

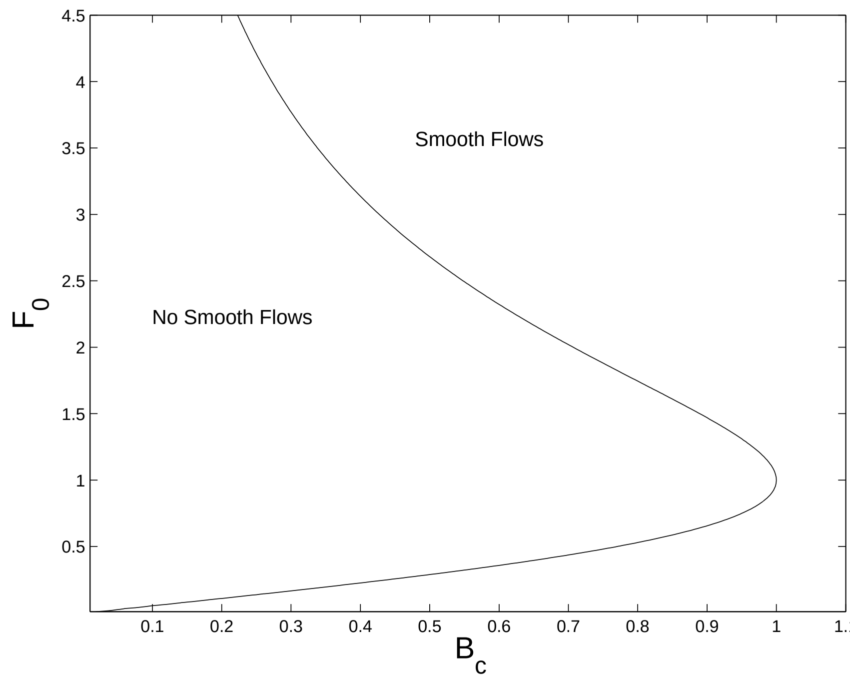

Figure 5: The smooth solution boundary is plotted in the B_cF_0-plane, where B_c is the nondimensional contraction width, and F_0 is the ratio of the flow speed to the characteristic flow rate of the fluid. We note that $B_c = 1$ corresponds to a blocked flow and $B_c = 1$ corresponds to a straight channel.

The stationary points of this cubic are at $H = 0$ and $H^* = \frac{2}{3}(\frac{1}{2}F_0^2 + 1)$. Now since physically meaningful roots exist only for $H > 0$, we can determine when there are positive roots by evaluating $P(H)$ at $H = H^*$. When $p(H^*) <= 0$ there are positive roots, and when $p(H^*) > 0$ there are no positive roots. Thus the point $p(H^*) = 0$ determines the boundary between smooth and nonsmooth solutions in the B_cF_0-plane. This is a standard technique in hydraulic theory [7]. We obtain

$$\frac{3}{2}\left(\frac{F_0}{B_c}\right)^{2/3} - (1 + \frac{1}{2}F_0^2) = 0. \tag{12}$$

Figure 5 illustrates how for a given geometry B_c and incoming depth h_0 there is a maximum speed at which a subcritical smooth flow can pass. It is also interesting to note that for channels with expanding width $B > 1$ we can find a smooth flow regardless of the speed. In the next section we will look at non-smooth flows.

3.3 Upstream Moving Bores

Here we will look for solutions with a discontinuity, or jump, at one point. We will allow this jump to move upstream at speed s, where s is positive when moving to the left, as in Figure 6.

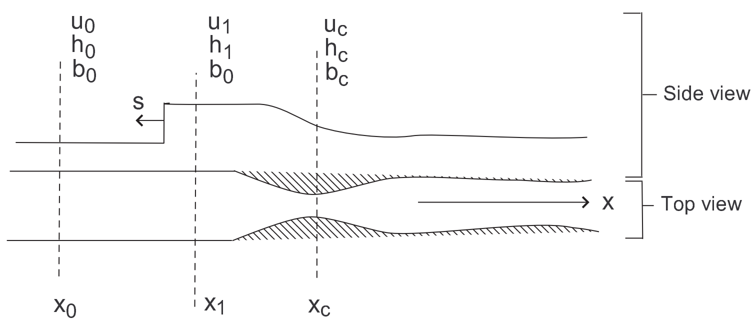

Figure 6: Both the free surface profile and the planar view are shown. Here we have a shock moving upstream with speed s. Conservation laws will be used to couple the fluid motion between points x_0, x_1, and x_c.

As in Figure 6, we will pick a point upstream, x_0, one between the jump and the nozzle, x_1, and the point of minimum width at the nozzle, x_C. We will label the width, height, and velocity at these points with subscripts that match the respective points. The goal is to find in which regions of the B_cF_0-plane there exist shock solutions. We can couple the flow at points x_1 and x_C using Bernoulli's equation (13c) and conservation of mass (13b) as before. The flow at points x_0 and x_1 can be coupled by conservation of mass in the frame of the jump (13a) and a jump condition (13d) which we can derive from the conservative form of the momentum equation. Consequently, we have four equations for five unknowns, so we impose the restriction that flow is critical (13e) at the nozzle, and obtain the system

$$\begin{aligned}
(u_0+s)h_0b_0 &= (u_1+s)h_1b_1 && (13a)\\
u_1h_1b_1 &= u_ch_cb_c && (13b)\\
\frac{1}{2}u_1^2+gh_1 &= \frac{1}{2}u_c^2+gh_c && (13c)\\
(u_0+s)^2 &= \frac{gh_1}{2}(1+\frac{h_1}{h_0}) && (13d)\\
u_c^2 &= gh_c. && (13e)
\end{aligned}$$

Taking a critical condition at the nozzle is a common assumption in hydraulics. It is equivalent to imposing the restriction that there are no waves at infinity [5]. Now, we have a system of five equations for five unknowns u_1, u_c, h_c, h_1, s, with parameters $h_0, u_0, b_1 = b_0, b_c$. Nondimensionalizing $B = b_c/b_0, F_0 = u_0/\sqrt{gh_0}, H_1 = h_1/h_0, S = s/\sqrt{gh_0}$, system (13) simplifies to

$$\begin{aligned}
\frac{1}{2}\left(F_0+(1-H_1)S\right)^2 &= \frac{3}{2}H_1^2\left(\frac{F_0+(1-H_1)S}{B_c}\right)^{2/3}-H_1^3 && (14a)\\
(F_0+S)^2 &= \frac{1}{2}H_1(1+H_1). && (14b)
\end{aligned}$$

Figure 7 shows the region of the B_cF_0-plane where (14) has physically meaningful solutions. This region was obtained by first fixing H_1 and then finding the solution curves for S and then fixing S and finding the solution curves for H_1. The boundaries correspond to smooth flow $H_1 = 1$ and steady shocks $S = 0$.

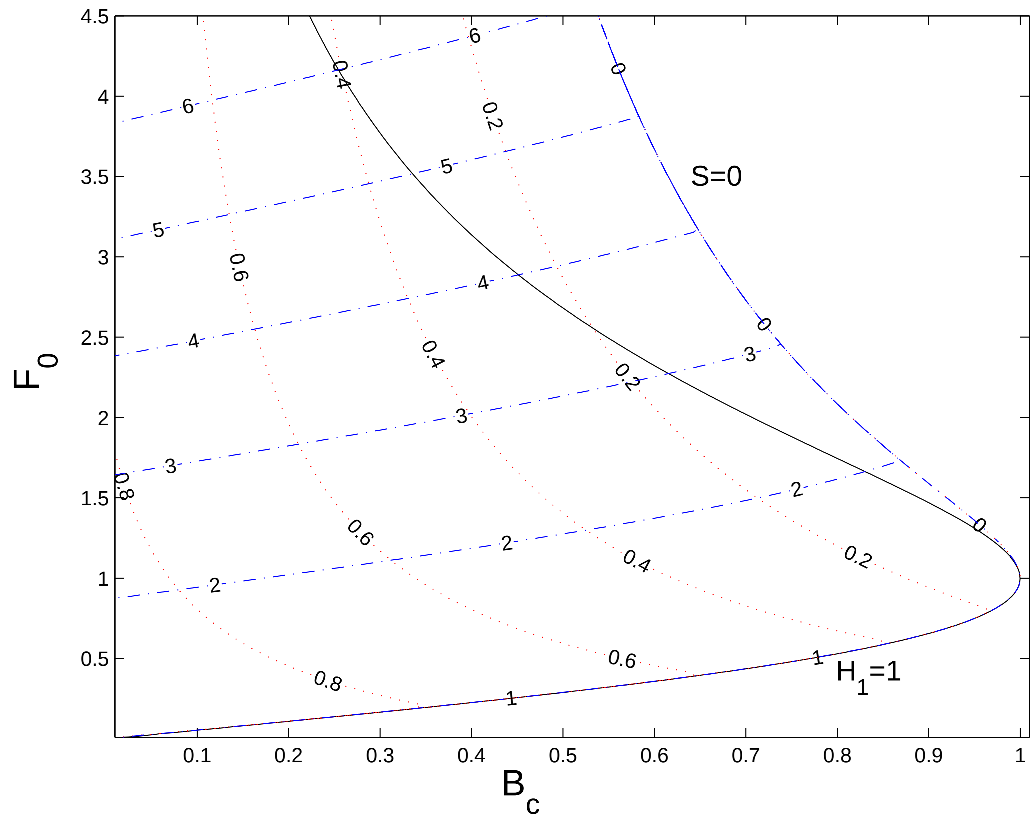

Figure 7: The level sets of the shock speed (dotted lines) and height ratio (dashed lines) are plotted. The solid line is the smooth solution boundary. Notice there is a wedge where there are both smooth and moving shock solutions.

3.4 Hydraulic Jumps in the Contraction

Here we examine for which flow rates F_0 and contraction widths B_c there can be steady shocks. Steady shocks in a contraction are solutions to

$$\begin{aligned}
u_0h_0b_0 = u_1h_1b_1 &= u_2h_2b_1 = u_ch_cb_c && (15a)\\
\frac{1}{2}u_0^2 + gh_0 &= \frac{1}{2}u_1^2 + gh_1 && (15b)\\
\frac{1}{2}u_2^2 + gh_2 &= \frac{1}{2}u_c^2 + gh_c && (15c)\\
u_1^2 &= \frac{gh_2}{2}(1 + \frac{h_2}{h_1}) && (15d)\\
u_c^2 &= gh_c. && (15e)
\end{aligned}$$

These seven equations are mass and momentum balance between four locations plus the critical condition. The four locations are the far upstream, h_0, u_0, b_0, the upstream limit of the shock u_1, h_1, b_1, the downstream limit h_2, u_2, b_1, and the nozzle u_c, h_c, b_c. If we nondimensionalize as follows, $H_1 = h_1/h_0$, $H_2 = h_2/h_0$, $B_c = b_c/b_0$, then we can reduce (15) to

$$\begin{aligned}
\frac{1}{4}H_2^2 - (\frac{1}{2}F_0^2 + 1)H_1 + \frac{1}{4}H_1H_2 + H_1^2 &= 0 && (16a)\\
H_2^2 - \frac{3}{2}(\frac{F_0}{B_c})^{2/3}H_2 + \frac{1}{4}H_1H_2 + \frac{1}{4}H_1^2 &= 0. && (16b)
\end{aligned}$$

We will use (16) to find where in the F_0B-plane we have steady shocks. A simple way to do this is to consider what the boundaries of this region should be. If we have a shock we know from the energy condition that $H_1 \leq H_2$ [3]. Now if we look at where this upper bound on H_1 is satisfied with equality $H_1 = H_2$, we can then reduce (16) to

$$\frac{1}{2}F_0^2 + 1 - \frac{3}{2}(\frac{F_0}{B_c})^{2/3} = 0, \tag{17}$$

which is the boundary (12) of smooth solutions we already determined. This boundary came from considering an upper bound on H_1. The other boundary should then come from a lower bound. Since we are working here with supercritical flow in a contracting region, we expect H_1 to grow the farther we move into the contraction. Thus the other boundary should be when the shock is at the mouth of the contraction, or when $H_1 = 1$. Substituting this into equations ($16a$) and ($16b$) yields

$$5 + 16F_0^2 + 6(\frac{F_0}{B_c})^{2/3} - 3\sqrt{1 + 8F_0^2} - 6(\frac{F_0}{B_c})^{2/3}\sqrt{1 + 8F_0^2} = 0. \tag{18}$$

This is the limiting curve we found for moving shocks when the speed goes to zero. Thus we have steady shocks in the contraction only in the wedge of Figure 7 where we had both smooth solutions and upstream moving shocks.

Next we examine the stability of steady shocks. Consider a system with a steady shock in the contraction region, with u_1 and h_1 the upstream limit of the velocity and height at

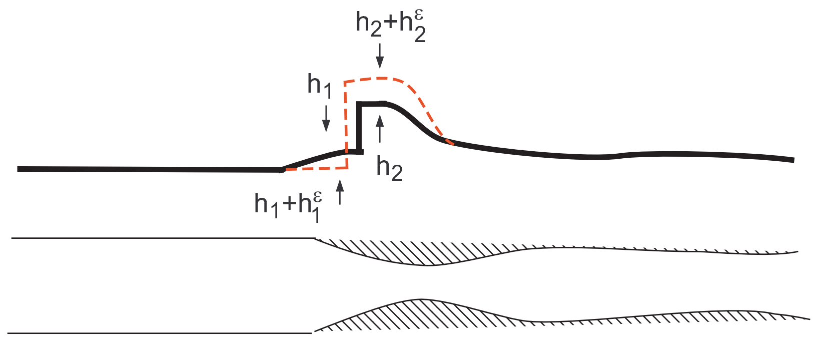

Figure 8: Sketch of the unperturbed solution (solid curve) juxtaposed over the perturbed shock (dashed curve).

the shock and u_2, h_2 the downstream limit. Now we will assume a small perturbation which generates a shock moving at a small speed s, see Figure 3.4.

Let us present equations which govern the perturbed flow. The perturbations are denoted with a superscript ϵ. The perturbed flow balances mass and momentum over the shock

$$
\begin{aligned}
(u_1 + u_1^\epsilon + s)(h_1 + h_1^\epsilon) &= (u_2 + u_2^\epsilon + s)(h_2 + h_2^\epsilon) &(19)\\
(u_1 + u_1^\epsilon + s)^2(h_1 + h_1^\epsilon) + \frac{g}{2}(h_1 + h_1^\epsilon)^2 &= (u_2 + u_2^\epsilon + s)^2(h_2 + h_2^\epsilon) + \frac{g}{2}(h_2 + h_2^\epsilon)^2. &(20)
\end{aligned}
$$

Mass will be conserved upstream of the jump

$$(u_1 + u_1^\epsilon)(b + b^\epsilon)(h_1 + h_1^\epsilon) = Q. \tag{21}$$

We will assume that the perturbation does not affect the far field momentum upstream E_1 or downstream E_2, so the Bernoulli constants are unchanged

$$\frac{1}{2}(u_1 + u_1^\epsilon)^2 + g(h_1 + h_1^\epsilon) = E_1 = \frac{1}{2}u_1^2 + gh_1 \tag{22}$$

$$\frac{1}{2}(u_2 + u_2^\epsilon)^2 + g(h_2 + h_2^\epsilon) = E_2 = \frac{1}{2}u_2^2 + gh_2. \tag{23}$$

Now we assume that we have a small perturbation and small resulting shock speed. Linearizing all these equations gives a linear system of six unknowns and five equations

$$
\begin{aligned}
u_1^\epsilon h_1 b + u_1 h_1 b^\epsilon + u_1 b h_1^\epsilon &= 0 &(24a)\\
u_1^\epsilon h_1 + s h_1 + u_1 h_1^\epsilon - u_2^\epsilon h_2 - s h_2 - u_2 h_2^\epsilon &= 0 &(24b)\\
2h_1 u_1(u_1^\epsilon + s) + h_1^\epsilon u_1^2 + g h_1 h_1^\epsilon - 2h_2 u_2(u_2^\epsilon + s) - h_2^\epsilon u_2^2 - g h_2 h_2^\epsilon &= 0 &(24c)\\
u_1 u_1^\epsilon + g h_1^\epsilon &= 0 &(24d)\\
u_2 u_2^\epsilon + g h_2^\epsilon &= 0. &(24e)
\end{aligned}
$$

The goal is to reduce this to a single equation for the perturbed shock speed s in terms of the change in channel width b^ϵ. If b^ϵ and s have opposite signs and we are in a contraction, then the solution is stable, because the shock speed will force the shock back to its previous

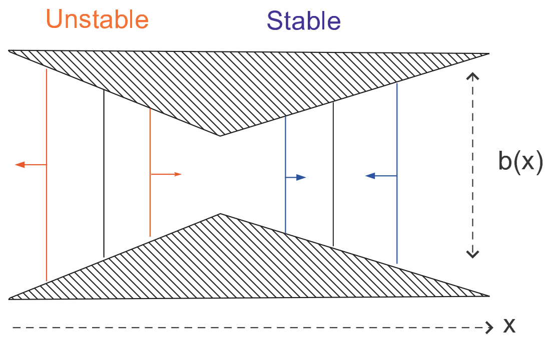

Figure 9: A sketch of the contraction region as viewed from above. The solid vertical lines denote shocks. In a contracting region steady shocks are unstable, while in a dilation they are stable.

position. If instead they have the same sign, then it is unstable, because the shock will propagate away from its previous location, as shown in Figure 9.

After some algebra we obtain the relationship

$$S = \frac{F_1(1 - \frac{u_1}{u_2})}{(1 - \frac{h_2}{h_1})} B^\epsilon. \tag{25}$$

Here $S = s/\sqrt{gh_1}$ and $B^\epsilon = b^\epsilon/b_0$. We know that across a physical shock, $h_2 > h_1$ and also that $u_2 < u_1$, so this gives that sign(S)=sign(B^ϵ). Details of the above calculation are found in an appendix to this work [1].

4 Results

Experiments were conducted over a variety of flow speeds and channel geometries. In each experiment, the contraction width B_c was set and then the flow rate Q was varied. The inflow height was kept fixed for all experiments at $h_0 = 1.3cm$. The upstream channel width was also a constant $b_0 = 20cm$. For each flow rate we recorded the category of the flow, either smooth flow, moving shock, steady shock, or oblique shock. These flow state are depicted in Figure 10. For moving shocks the speed and height ratios across the shock were measured. There is an experimental difficulty, in that we cannot measure the speed of fast moving shocks. When measuring a flow, there is a time delay between when we initiate the flow and when it reaches a steady state. In this experiment the time delay is on the order of five seconds. Thus for flows with shock speeds larger than 15 cm/sec, the shock will move to the end of our channel before we can properly measure the speed. The data for the moving shocks where we could measure both the speed and the height are found in Table 1.

In addition to measuring the speed of moving shocks, we also took measurements when we had oblique shocks in the flow. Oblique shocks are a stationary phenomena in our flow,

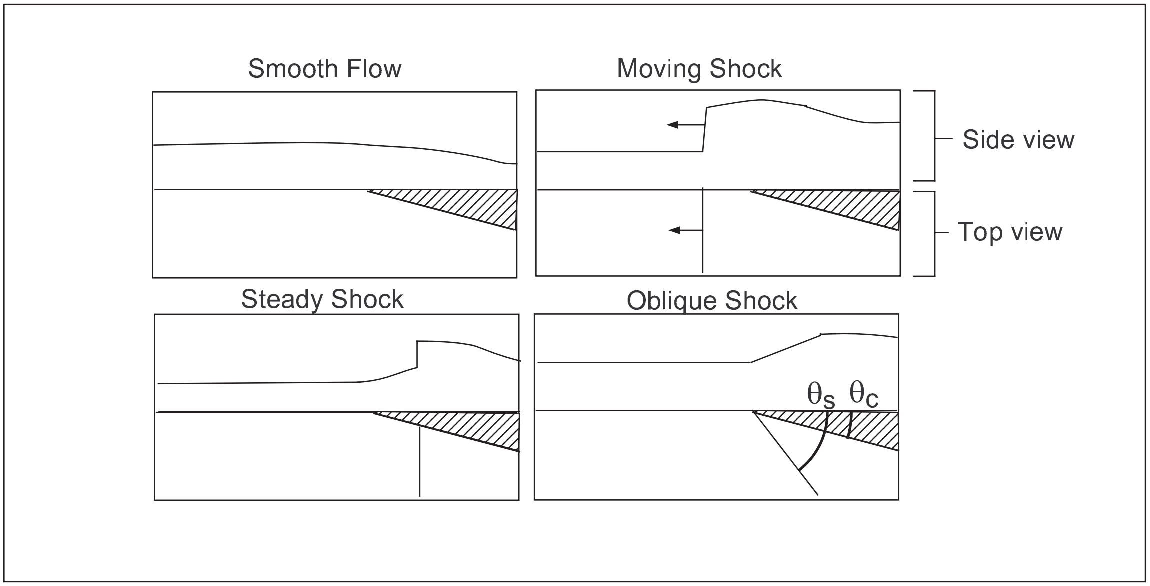

Figure 10: Shown are sketches of the four types of flow behavior. Each sketch shows a profile of the flow and a planar view.

$B_c = b_c/b_0$	$F_0 = u_0/\sqrt{gh_0}$	$H_1 = h_1/h_0$	$S = s/\sqrt{gh_0}$
0.6	3.19	3.54	0.15
0.6	3.55	3.77	0.08
0.7	2.31	2.54	0.11
0.7	2.40	2.85	0.19
0.7	2.49	2.69	0.05
0.7	2.80	3.08	0.08
0.7	2.98	3.23	0.02
0.8	2.10	2.31	0.08
0.81	2.20	2.62	0.09
0.875	2.07	2.23	0.06

Table 1: The experimental data for moving shocks are presented here. B_c is the nondimensional contraction ratio; F_0 the upstream Froude number; H_1 the nondimensional height ratio across the shock; and S the nondimensional shock speed.

so we do not have the difficulty of measuring speed as in the moving case. There is a new difficulty. When oblique shocks are very weak, surface tension effects will become important, and rather than a shock, we see capillary waves in our contraction region. A picture of this phenomena is shown in Figure 11.

Figure 11: Weak shocks can be distorted by capillary waves.

Since we only want to measure oblique shocks, we need a criterion to determine when we have an oblique shock and when we have capillary waves. The criteria used here is that when there is a measurable height difference between the fluid upstream and downstream of the front, we call it an oblique shock. When the mean fluid height is the same on both side of the front we call it a capillary wave. The data from the oblique shocks we measured are presented in Table 2.

$H_1 = h_1/h_0$	$F_0 = u_0/\sqrt{gh_0}$	θ_c	θ_s
1.9	2.79	9.5	26.7
1.5	2.94	3.8	26.7
1.7	3.13	9.5	27.1
1.5	3.32	3.8	21.6
1.5	3.37	5.7	22.1
1.9	3.47	7.6	25.4
1.7	3.56	9.5	20.1
1.8	3.65	7.6	25.2

Table 2: The experimentally measured flow variables for the oblique shocks are presented here. H_1 is the nondimensionalized height ratio across the shock, F_0 is the upstream Froude number, θ_c is the angle of the contraction, θ_s is the angle of the shock, see also Figure 10.

We measured the flow rate and geometry for every experiment. The different flow types are plotted in the $B_c F_0$-plane in Figure 12.

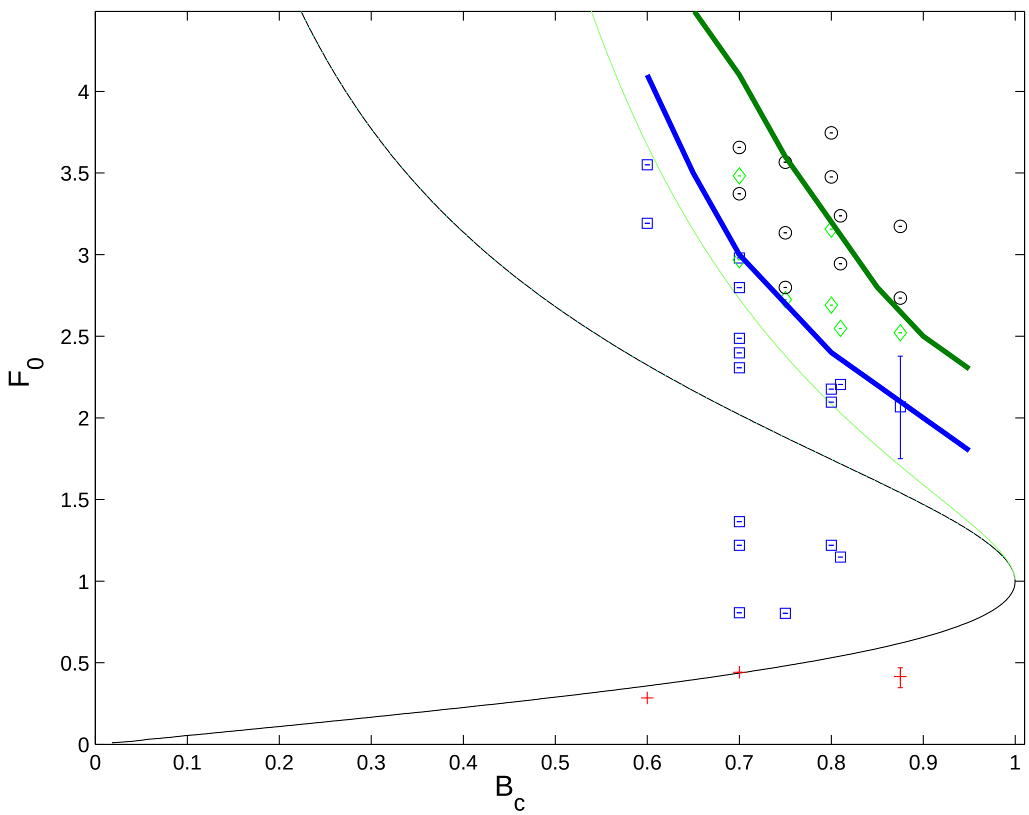

Figure 12: Experiments plotted in the predicted inviscid state space. Here circles are oblique shocks, diamonds are steady shocks, squares are moving shocks, pluses are smooth flows. Representative error bars are plotted on a smooth flow and a moving flow at $B_c = 0.875$. The thick lines are the numerically computed boundaries for the regions where an upstream moving shock can be stopped via friction.

5 Discussion

In this section we will compare the experimental results to mathematical theory. The models used in this report assume no effects of surface tension or viscosity. The importance of these effects are commonly measured using nondimensional numbers, Weber We for surface tension and Reynolds Re for viscosity. Table 3 shows the range for these parameters in the experiments considered.

Parameter	**Min**	**Max**
Reynolds ($Re = UL/\nu$)	1,300	20,100
Weber ($We = \rho U^2 L/\sigma$)	1.85	433
Froude ($F_0 = U_0/\sqrt{gh_0}$)	0.28	4.34
Contraction ($B_c = b_c/b_0$)	0.6	0.875

Table 3: The nondimensional parameters are estimated for the main body of our flow. Here $We \approx 14F_0^2$ and $Re \approx 3300F_0$. If we look at some local phenomena, for instance near weak oblique shocks, we can have smaller Weber and Reynolds numbers.

If we look at Equation (14) we see that for a given upstream Froude number F_0 and nondimensional shock speed S, we can predict the height ratio across the shock. We can then compare this prediction to the measured height ratios across the jump. This comparison is shown in Figure 13.

5.1 Oblique Shocks

All the analysis at the beginning of this report considered only 1-D phenomena. Oblique shocks are a two-dimensional (2-D) phenomena, so our model does not take them into account. Following [2] and [8], we can derive a system of equations for the oblique shock angle θ_s and shock height h_1. These equations will allow us to predict θ_s and h_1 given the upstream conditions h_0, F_0 and the angle of the contraction θ_c, as follows

$$\frac{h_1}{h_0} = \frac{\tan\theta_s}{\tan(\theta_s - \theta_c)} \tag{26a}$$

$$\sin\theta_s = \sqrt{\frac{1}{2\,F_0^2}\,\frac{h_1}{h_0}\,(1 + \frac{h_1}{h_0})}. \tag{26b}$$

Using (26) we can plot our predicted oblique shock angles against the experimental ones. This plot is shown in Figure 14.

In our experiments we saw oblique shocks that exit our channel before interacting with another shock, and oblique shocks that intersect in the channel, see Figure 15. A similar calculation was also done which can be used to predict the angles of intersecting oblique shocks.

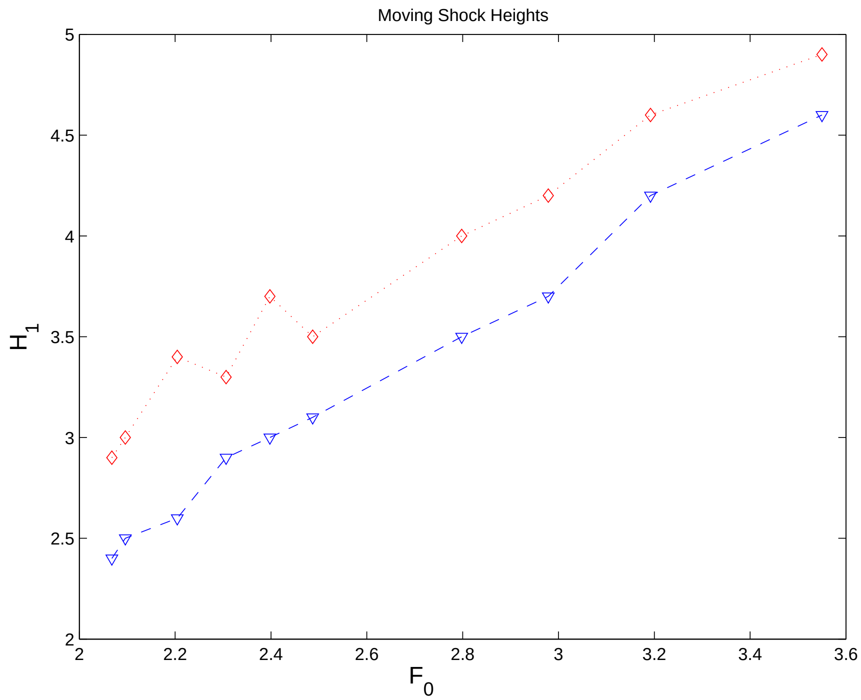

Figure 13: The experimental height ratios are plotted against the inviscid predictions. The dotted curve (diamonds) corresponds to the experimental measurements; the dashed curve (triangles) to the inviscid predictions. The experimental measurements are systematically lower than the predicted curve due to the effect of friction.

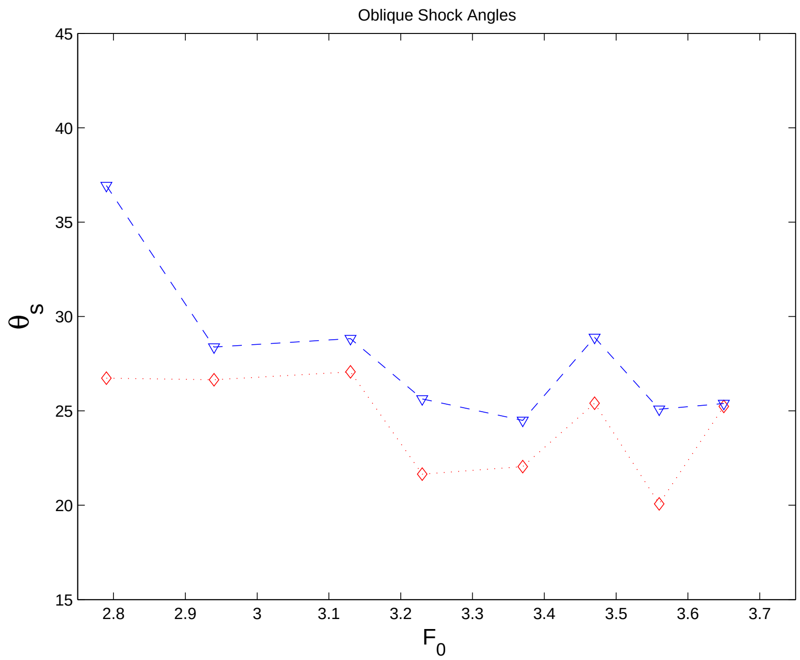

Figure 14: The observed oblique shock angles (diamonds, dotted curve) are plotted against the calculated angles (triangles, dashed curve).

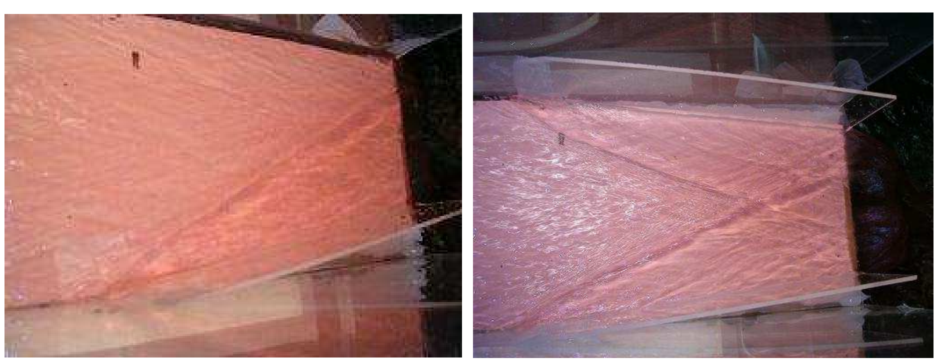

Figure 15: The left image is a single oblique shock in an asymmetric contraction, $F_0 = 3.56, B_c = 0.75$. The right image shows the intersection of two oblique shocks in a symmetric contraction, $F_0 = 3.65, B_c = 0.7$.

5.2 Turbulent Drag

If we examine Figure 12 we see that there are steady shocks outside of the region predicted by the inviscid theory. To explain this, we must reexamine the assumptions of the original model. The real fluid does have some viscosity, so we should take this into account. In the hydraulic equations, viscous effects are usually added with a drag term. The most physical drag term comes from a quadratic drag law [3]. Adding such a term changes the hydraulic equations (6) to the system

$$uu_x + gh_x = -C_d u^2/h \tag{27a}$$
$$(buh)_x = 0. \tag{27b}$$

This system of ordinary differential equations (ODE's) can now be solved using standard numerical techniques. When we do not have smooth solutions we can find steady shocks by using the inflow conditions at the sluice gate and critical condition at the nozzle as boundary conditions to march the solutions together until they match with a shock.

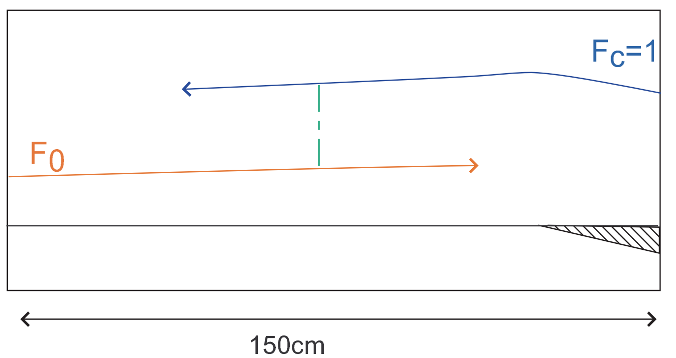

Figure 16: A cartoon of the numerical method for finding steady shocks. We use an ODE solver to find the smooth flow with a prescribed upstream Froude number F_0 and the smooth flow that meets the critical condition $F_c = 1$. These two smooth flows are then matched using the shock condition.

Depending on the Froude number F_0 and geometry B_c, we may or may not be able to have a steady shock of this type. If we solve this system throughout our state space we get numerically computed boundaries for when we can have steady shocks with friction. These boundaries are plotted in Figure 12. For our computations we have used $C_d = 0.004$ [4].

5.3 Multiple States

In our inviscid calculations, we predicted a region in the B_cF_0-plane where we can have three different steady states: steady shocks, moving shocks, and supercritical smooth flows. We have shown that the steady shocks in the contraction region are unstable, so we don't expect to see these. We also have observed that friction can stop slowly moving shocks, and that supercritical smooth flows correspond to oblique shocks. Thus this region of multiple states really corresponds to flow speeds where we can have upstream steady shocks, stopped via friction, and oblique shocks in the contraction region. These phenomena were observed in the lab. Figure 12 shows both oblique shocks and steady shocks in the same region of state space. We also observed that large perturbations of these flows can cause the flow to change from one steady state to another. If we have a steady upstream shock, we can physically push most of the water that is behind the shock out of the channel, and see a steady oblique shock. If we have an oblique shock, we can block the flow for a small time period, and the resulting flow will evolve into a steady upstream shock. Figure 17 shows snapshots of the transition from oblique shocks to an upstream steady shock.

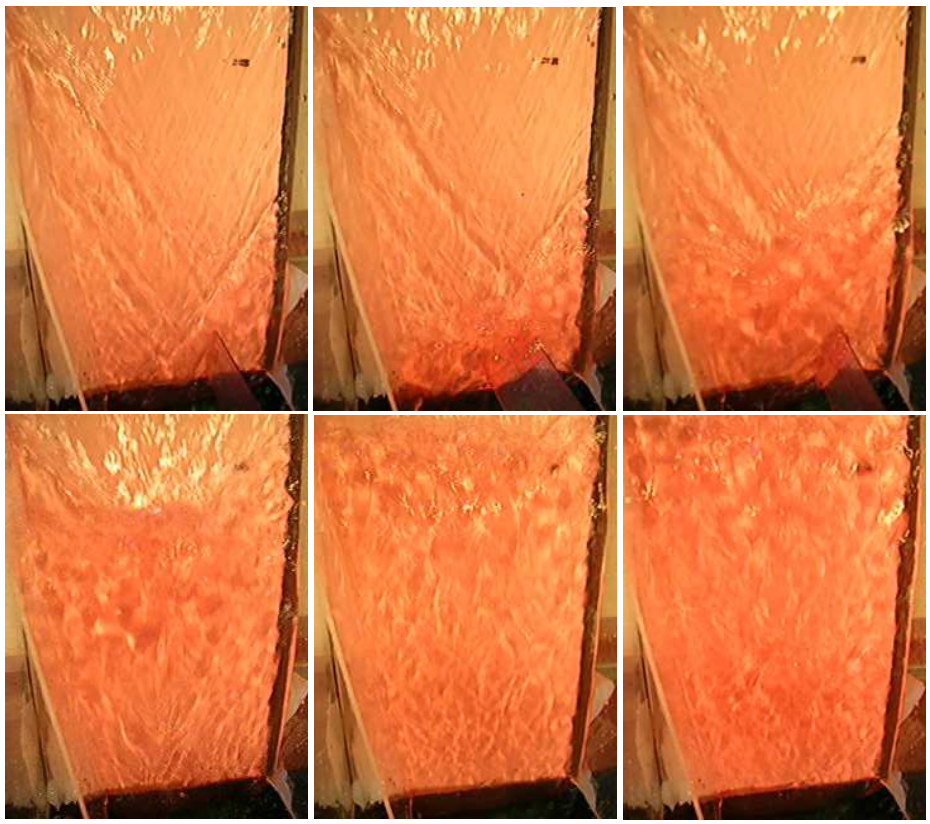

Figure 17: Shown are snapshots of the flow transition from oblique shocks to a steady upstream shock. The time interval between each frame is 1 second. Here we have the Froude number $F_0 = 2.8$ and the contraction ratio $B_c = 0.7$. A ruler is used to restrict the flow for a small time period to induce this state change.

6 Conclusion and future work

We presented a mathematical and experimental investigation into shallow water flow through a contraction. We began by making predictions using a simple 1-D inviscid theory. We saw that for slow speeds this 1-D analysis performs well. For higher speeds boundary drag becomes important and we saw a departure from the 1-D inviscid predictions. The addition of drag forces improved the performance of the 1-D theory. To predict oblique shocks, a fundamentally 2-D feature, we had to use the 2-D shallow water equations.

We also set out to investigate the existence and stability of steady shocks. We presented a perturbation method for finding when steady shocks in the contraction are stable. Experimentally we observed that shocks which are stopped via friction are stable. If we look at how the shock speed depends on flow rate, see Figure 7, we see that there is a heuristic stability result which agrees with our predictions and observations. When the flow rate is increased, shocks move slower, and when the flow rate is decreased shocks move faster. If we apply this knowledge to a steady shock, we see that in accelerating flows, steady shocks will be unstable. If we displace a steady shock upstream in an accelerating flow it will have a faster speed, and will move upstream. Also downstream displacements will generate slower speeds, and the shocks will move downstream. A similar argument shows that in decelerating flows steady shocks are stable. This argument is incomplete however, in that it does not deal with flows where the velocity is not monotone. This is precisely the case of a steady shock in a contraction, so here we used the perturbation method of [4].

There are a variety of avenues for future research illuminated by the experiments and analysis presented here. First, we have observed that supercritical flows that are 1-D smooth have additional 2-D shock structure which is not accounted for with 1-D theory. In the appendices of this report [1] we have predictions for some of these 2-D structures. We also observed a structure like a Mach stem near the intersection of two oblique shocks. This structure has not been accounted for in the work presented in this report. Another avenue for future research is to use this work in conjunction with [2] as a base for investigating shallow flow of composite media, i.e. water carrying sediment. Also this report does not include analysis of the time dependent problem. Here we could investigate the relationship between initial data and steady state in the region of multiple steady states. Future work is currently being done to compare 2-D simulations with experimental results. A few experiments have been done on Mach stems and adding polystyrene beads to simulate granular media. For updates on the current state of the work, see http://www.math.wisc.edu/∼akers/contraction.

7 Acknowledgements

This work was funded via a summer fellowship from the Geophysical Fluid Dynamics Program at the Woods Hole Oceanographic Institution. Thanks are due to Larry Pratt and Jack Whitehead for valuable discussions. Keith Bradley was instrumental in the construction and design of the tank where the experiment was conducted. Also a special thank you to Onno Bokhove for the inspiration and guidance of this project.

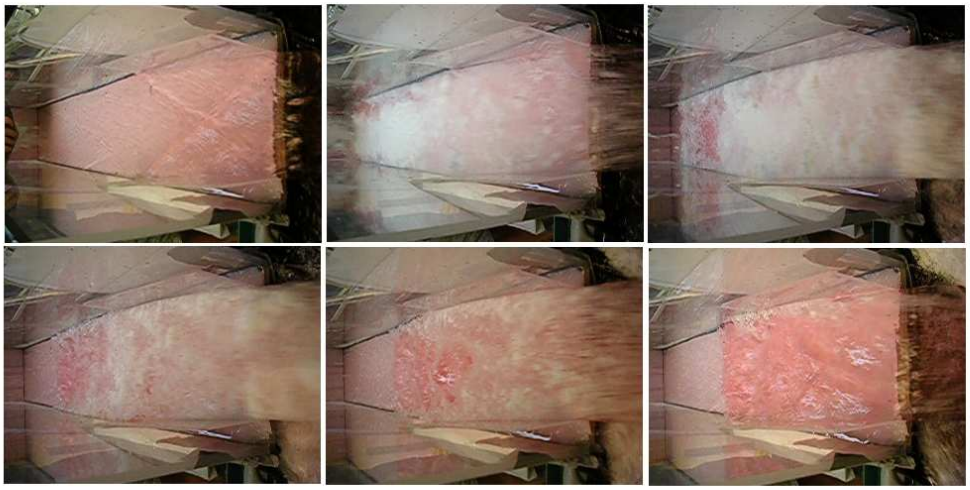

Figure 18: Here are snapshots of an experiment where polystyrene beads are impulsively dumped into a flow that exhibits three states: upstream shocks, Mach stems, and oblique shocks. The flow begins in the state of oblique shocks, with $F_0 = 3.08, B_c = 0.7$. Beads are dumped into the flow, and the resulting flow is an upstream shock.

References

[1] B. Akers, *Oblique and steady shock calculations*, 2005. Appendix, available upon request.

[2] M. Al-Tarazi, O. Bokhove, J. Kuipers, M. van Sint Annaland, and A. W. Vreman, *Reservoir formation in shallow granular flows through a contraction*, Physical Review Letters, (Under Revision).

[3] P. Baines, *Topographical effects in stratified flows*, Cambridge University Press, 1995.

[4] P. Baines and J. Whitehead, *On multiple states in single layer flows*, Physics of fluids, (2003).

[5] J. Keller, *Personal communication*, 2005.

[6] K. Muller, *Tsunami-like river tides are surfing's new frontier*, National Geographic, (2005).

[7] L. Pratt, C. Hills, and J. Parsons, *Review of hydraulics for non-rotating 1-d single layer flows*, tech. rep., Woods Hole Oceanographic Institution: Geophysical Fluid Dynamics Program, 1997.

[8] A. Shapiro, *The Dynamics and Thermodynamics of Compressible Fluid Flow*, The Ronald Press Company, 1954.

[9] G. B. Whitham, *Linear and Nonlinear Waves*, Wiley-Interscience, 1999.